Synchronization transition of heterogeneously coupled oscillators on scale-free networks

E. Oh,[1] D.-S. Lee,[2] B. Kahng,[1,3] and D. Kim[1]
[1]*CTP & FPRD, School of Physics and Astronomy, Seoul National University, Seoul 151-747, Korea*
[2]*Theoretische Physik, Universität des Saarlandes, 66041 Saarbrücken, Germany*
[3]*Center for Nonlinear Studies, Los Alamos National Laboratory, Los Alamos, New Mexico 87545, USA*
(Received 1 June 2006; published 10 January 2007)

We investigate the synchronization transition of the modified Kuramoto model where the oscillators form a scale-free network with degree exponent λ. An oscillator of degree k_i is coupled to its neighboring oscillators with asymmetric and degree-dependent coupling in the form of $Jk_i^{\eta-1}$. By invoking the mean-field approach, we find eight different synchronization transition behaviors depending on the values of η and λ, and derive the critical exponents associated with the order parameter and the finite-size scaling in each case. The synchronization transition point J_c is determined as being zero (finite) when $\eta>\lambda-2$ ($\eta<\lambda-2$). The synchronization transition is also studied from the perspective of cluster formation of synchronized vertices. The cluster-size distribution and the largest cluster size as a function of the system size are derived for each case using the generating function technique. Our analytic results are confirmed by numerical simulations.

DOI: 10.1103/PhysRevE.75.011104 PACS number(s): 05.70.Fh, 89.75.Hc, 05.45.Xt

I. INTRODUCTION

Synchronization of oscillations is one of the fundamental nonlinear phenomena in biology, physics, chemistry, communication science, and many other branches of science and engineering [1]. Recently, the dynamics of synchronization of oscillators located at each vertex in complex networks has attracted much attention. That is because the small-world feature of complex networks is closely related to their synchronizability. By the small-world feature, we mean that the average separation $\langle d\rangle$ between a pair of vertices scales at most $\langle d\rangle \sim \ln N$, where N is the number of vertices in the system. It was shown [2,3] that the stability of a completely synchronized state is significantly enhanced in the small-world network model introduced by Watts and Strogatz [4], compared with random networks. However, such a feature is not observed in scale-free (SF) networks. SF networks are the networks that exhibit a power-law degree distribution $P_d(k)\sim k^{-\lambda}$ and the degree k is the number of edges connected to a given vertex [5]. In SF networks, the heterogeneity in the degree distribution suppresses their synchronizability in a completely synchronized state [6]. Thus, it was desired to introduce a dynamic model [7] that prompts SF networks to be more synchronizable. Moreover, it was shown [8,9] that synchronizability is more enhanced in weighted complex networks.

The dynamics of synchronization is described by various forms of coupled equations. A linearly coupled model is probably the simplest one. In the model, N oscillators are coupled when they are connected via edges. The coupling constant is normally symmetric; however, it is not necessarily symmetric to achieve a better synchronizability. This case can happen in SF networks: It was shown recently [7] that the synchronizability becomes maximum when information flow diffuses and reaches a uniform stationary state over the entire system. Here, the mapping from synchronization dynamics to information flow can be naturally introduced, because the linearly coupled equation is nothing but the diffusion equation. It was shown [7] that the uniform-stationary state can be reached by introducing asymmetric and weighted coupling strength between a pair of vertices or oscillators.

To be specific, the dynamic model with the asymmetric coupling strength is written as

$$\frac{d\phi_i}{dt} = f(\phi_i) - \frac{J}{k_i^{1-\eta}}\sum_{j=1}^{N} a_{ij}[h(\phi_i) - h(\phi_j)] \tag{1}$$

for $i=1,\ldots,N$. Here, ϕ_i is the phase of an oscillator located at vertex i, $f(\phi)$ describes the dynamics of an individual oscillator, and J is the overall coupling strength. k_i is the degree of vertex i, and a_{ij} is an element of the adjacent matrix, which is 1 if vertices i and j are connected and 0 otherwise. $h(\phi_i)$ is the output function and takes a form of $h(\phi_i)=\phi_i$ for the linear case. It is noteworthy that the coupling strength of Eq. (1) is asymmetric and weighted due to the factor $1/k_i^{1-\eta}$ unless $\eta=1$. When $\eta>0$, vertices with a large degree can influence other vertices significantly on regulating phases due to their large numbers of connections; on the other hand, when $\eta<0$, the influence is reduced. It was found [7] that the system is most synchronizable when $\eta=0$, irrespective of the value of the degree exponent of a given SF network.

In this paper, we study a different issue of synchronization problems: the behavior of the synchronization transition from a desynchronized to a synchronized state near the critical point. For this purpose, we use the Kuramoto model [10] with modified coupling strength as appears in Eq. (1): that is,

$$\frac{d\phi_i}{dt} = \omega_i - \frac{J}{k_i^{1-\eta}}\sum_{j=1}^{N} a_{ij}\sin(\phi_i - \phi_j). \tag{2}$$

The oscillators are located at each vertex $i=1,\ldots,N$ of a SF network with degree exponent λ. Here, ω_i is the natural frequency of the ith oscillator selected from the Gaussian distribution $g(\omega)=e^{-\omega^2/2}/\sqrt{2\pi}$. We find that the modified Kuramoto dynamic model displays a very complex and rich behavior in the space of the two tunable parameters (η,λ).

The synchronization transition from a desynchronized to a synchronized state occurs at the critical point J_c. For small $J \ll J_c$, the coupling strength is so weak that an individual vertex maintains its own phase different from others; therefore, the entire system is desynchronized. As the coupling strength J increases, a cluster of vertices is more likely to be coupled, to be in a common or almost the same phase, and thus form a cluster of synchrony. The size of such clusters becomes diverse as the coupling strength J increases. At the critical point J_c, the system reaches a self-organized state and the cluster-size distribution follows a power law

$$n(s) \sim s^{-\tau} \tag{3}$$

in the thermodynamic limit. For $J \gg J_c$, the power-law behavior no longer holds and the entire system is synchronized.

The order parameter of the synchronization transition is defined as

$$re^{i\theta} = \frac{1}{N}\sum_{i=1}^{N} e^{i\phi_i}. \tag{4}$$

In the synchronized state, the phases ϕ_i of each vertex are narrowly distributed around an average phase θ. The amplitude r of the order parameter has a finite value; on the other hand, $r \approx 0$ in the desynchronized state. Thus, the exponent β associated with the order parameter is defined via the relation

$$r \sim \Delta^{\beta}, \tag{5}$$

where $\Delta = (J - J_c)/J_c$. In finite-size systems, the order parameter is described in terms of a scaling function as

$$r \sim N^{-\beta/\mu} \psi(\Delta N^{1/\mu}). \tag{6}$$

In recent works [11,12], the nature of the transitions and the finite-size scalings have been studied for the case of $\eta = 1$. In this work, we determine the order parameter and the size distribution of synchronized clusters for general η using the mean-field approach and the generating function technique. Moreover, we construct a finite-size scaling function for the order parameter and determine the exponent μ. Even for a simple extension of $\eta \neq 1$, we find that the obtained result is very rich. There exist eight distinct transition behaviors depending on the values of η and λ. Therefore, the result can be helpful in understanding diverse dynamic phenomena arising on SF networks.

The paper is organized as follows: In Sec. II, we first introduce and apply the mean-field approach to the dynamic equation (2). We construct a self-consistent equation for a local field and determine the order parameter. Next, the critical point is determined and the behavior of the order parameter near the critical point is obtained in Sec. III. The size distribution of synchronized clusters and the largest cluster size at the critical point are solved in Secs. IV and V, respectively. The finite-size scaling analysis for the order parameter is performed and the results are checked numerically in Sec. VI. A summary and discussion follow in Sec. VII.

II. ORDER PARAMETER EQUATION

In this section, we analyze the modified Kuramoto equation (2) in the framework of the mean-field approach by constructing a self-consistent equation for a local field. To proceed, we define $\bar{r}_i$ and $\bar{\theta}_i$ as the amplitude and phase of the local field at vertex i, respectively, via

$$\bar{r}_i e^{i\bar{\theta}_i} = \frac{1}{k_i}\sum_{j=1}^{N} a_{ij}\langle e^{i\phi_j}\rangle_t, \tag{7}$$

where $\langle \cdots \rangle_t$ denotes a time average. Then, Eq. (2) is rewritten in terms of the local field as

$$\frac{d\phi_i}{dt} = \omega_i - J\bar{r}_i k_i^{\eta} \sin(\phi_i - \bar{\theta}_i). \tag{8}$$

Here we ignore a term accounting for temporal fluctuations derived in [13]. The term can yield a different numerical value of the critical point in finite-size systems. However, in this paper, we mainly focus on the universal behavior of the critical exponents in the thermodynamic limit, thereby ignoring the term arising from the fluctuation effect. The fluctuation effect can change the critical point as studied in [13]. Once the amplitude $\bar{r}_i$ and the phase $\bar{\theta}_i$ of the local field are determined, one can solve Eq. (8) easily. The local field $\bar{r}_i$ is determined in a self-consistent manner.

We consider the probability density $\rho_i^{(s)}(\phi|\omega)d\phi$ that the phase of an oscillator i with natural frequency ω lies between ϕ and $\phi + d\phi$ in the steady state [14]. Using a previous result [14] that $\rho_i^{(s)}(\phi|\omega)d\phi$ is inversely proportional to the speed of ϕ, one can obtain that

$$\rho_i^{(s)}(\phi|\omega) = \begin{cases} \delta\left(\phi - \bar{\theta}_i - \sin^{-1}\left(\dfrac{\omega}{\omega_{*,i}}\right)\right) & \text{if } |\omega| \leq \omega_{*,i}, \\ \dfrac{\sqrt{\omega^2 - \omega_{*,i}^2}}{2\pi|\omega - \omega_{*,i}\sin(\phi - \bar{\theta}_i)|} & \text{otherwise,} \end{cases} \tag{9}$$

where $\omega_{*,i} = J\bar{r}_i k_i^{\eta}$. This result implies that an oscillator i with natural frequency ω has its phase locked at $\phi = \bar{\theta}_i + \sin^{-1}(\omega/\omega_{*,i})$ and $d\phi_i/dt = 0$ if $|\omega| \leq \omega_{*,i}$. Otherwise, its phase drifts with a finite speed, $d\phi_i/dt \neq 0$. Next, we can evaluate the order parameter using the stationary probability density in Eq. (9) as

$$re^{i\theta} = \frac{1}{N}\sum_i \int_{-\infty}^{\infty} d\omega g(\omega) \int d\phi \rho_i^{(s)}(\phi|\omega) e^{i\phi}. \tag{10}$$

Although $\bar{r}_i$, $\bar{\theta}_i$, and $\rho_i^{(s)}(\phi|\omega)$ can fluctuate over i in the steady state, we assume here that they depend only on degree k_i. This is a mean-field approximation. In general, the mean-field approximation is the first step used for studying diverse phase transition problems in Euclidean space and complex networks. Particularly, since SF networks are frequently locally tree like, the mean-field approximation works surprisingly for equilibrium problems such as the Ising model [15], the Ising spin-glass model [16], percolation [17], and so on. Also, it yields consistent results with numerical simulations for dynamic problems [18] at hand when $\lambda > 3$. Based on such background knowledge, here we invoke the mean-field approach for our study. Keeping only the degree-dependent

fluctuations, one can obtain a self-consistent equation for the local field through Eq. (7) as

$$\bar{r}(k)e^{i\bar{\theta}(k)} = \sum_{k'=1}^{k_m} P(k'|k) \int_{-\infty}^{\infty} d\omega g(\omega) \int_0^{2\pi} d\phi \rho^{(s)}(\phi|\omega,k') e^{i\phi}, \tag{11}$$

where $\rho^{(s)}(\phi|\omega,k)$ is given by the right-hand side of Eq. (9) with $\omega_*(k)=J\bar{r}(k)k^{\eta}$ replacing $\omega_{*,i}$. $P(k'|k)$ denotes the probability that a neighboring vertex of a given vertex with degree k has degree k', and k_m is the natural cutoff of degree. Here, we consider only the case that the network is random and does not have any type of degree-degree correlation; then, $P(k'|k)$ can be written as $k'P_d(k')/\langle k\rangle$ with $\langle k\rangle = \Sigma_k kP_d(k)$. After that, one can see that both $\bar{r}(k)$ and $\bar{\theta}(k)$ are independent of degree k, and therefore, we can drop the k dependence in $\bar{r}$ and $\bar{\theta}$ from now on.

The last integral of Eq. (11) is evaluated as

$$\int_0^{2\pi} d\phi \rho^{(s)}(\phi|\omega,k) e^{i\phi} = e^{i\bar{\theta}} \begin{cases} i[\omega/\omega_*(k)] - i\sqrt{[\omega/\omega_*(k)]^2 - 1} & [\omega > \omega_*(k)], \\ i[\omega/\omega_*(k)] + \sqrt{1 - [\omega/\omega_*(k)]^2}, & [|\omega| \leq \omega_*(k)], \\ i[\omega/\omega_*(k)] + i\sqrt{[\omega/\omega_*(k)]^2 - 1} & [\omega < -\omega_*(k)]. \end{cases} \tag{12}$$

The remaining integration in Eq. (11) for $\omega > \omega_*(k)$ and $\omega < \omega_*(k)$ cancels out due to the fact $g(\omega)=g(-\omega)$. As a result, only oscillators having frequency within the range $|\omega| \leq \omega_*(k)$ contribute to the local field in Eq. (7). Thus, one obtains

$$\bar{r} = \sum_{k=1}^{k_m} \frac{kP_d(k)}{\langle k\rangle} \int_{-\omega_*(k)}^{\omega_*(k)} d\omega g(\omega) \sqrt{1 - \left(\frac{\omega}{\omega_*(k)}\right)^2}, \tag{13}$$

which is the self-consistent equation for $\bar{r}$. Note that $\bar{r}$ is contained in $\omega_*(k)=J\bar{r}k^{\eta}$. After the local field is obtained, the order parameter in Eqs. (4) or (10) is calculated as

$$r = \sum_{k=1}^{k_m} P_d(k) \int_{-\omega_*(k)}^{\omega_*(k)} d\omega g(\omega) \sqrt{1 - \left(\frac{\omega}{\omega_*(k)}\right)^2}. \tag{14}$$

III. SYNCHRONIZATION TRANSITION

In this section, we solve the self-consistent equation (13) explicitly and then investigate the behavior of the order parameter near the critical point via Eq. (14). To proceed, we first recall that the degree distribution is given in a closed form as $P_d(k)=k^{-\lambda}/H_{k_m}^{\lambda}$ for $\lambda > 2$, where $H_{k_m}^{\lambda}$ is the generalized harmonic number, defined by $H_m^q \equiv \Sigma_{k=1}^m k^{-q}$ and $k_m \sim N^{1/(\lambda-1)}$. Substituting $g(\omega)=e^{-\omega^2/2}/\sqrt{2\pi}$ into Eq. (13), one can derive the local field $\bar{r}$ as

$$\begin{aligned} \bar{r} &= \sum_{k=1}^{k_m} \frac{kP_d(k)}{\langle k\rangle} \omega_*(k) \int_{-\pi/2}^{\pi/2} d\phi \cos^2\phi \frac{1}{\sqrt{2\pi}} e^{-[\omega_*(k)\sin\phi]^2/2} \\ &= \sum_{n=0}^{\infty} \frac{(n-1/2)!(-1)^n H_{k_m}^{\lambda-\eta-2n\eta-1}}{n!(n+1)!2^{n+3/2}H_{k_m}^{\lambda-1}} (J\bar{r})^{2n+1} \\ &\equiv \sum_{n=0}^{\infty} \bar{A}_n (J\bar{r})^{2n+1}, \end{aligned} \tag{15}$$

where we used the Taylor expansion of $e^{-[\omega_*(k)\sin\phi]^2/2}$ and the integration $\int_{-\pi/2}^{\pi/2} d\phi \cos^2\phi \sin^{2n}\phi = \pi^{1/2}(n-1/2)!/[2(n+1)!]$. Similarly, the order parameter is evaluated as

$$r = \sum_{n=0}^{\infty} \frac{(n-1/2)!(-1)^n H_{k_m}^{\lambda-\eta-2n\eta}}{2^{n+3/2}n!(n+1)!H_{k_m}^{\lambda}} (J\bar{r})^{2n+1} \equiv \sum_{n=0}^{\infty} A_n (J\bar{r})^{2n+1}. \tag{16}$$

If $\eta \leqslant 0$, the generalized harmonic numbers in $\bar{A}_n$ and A_n are finite, and then they can be represented in terms of the Riemann ζ functions for all n below and they are denoted as $\bar{B}_n$ and B_n, respectively: That is,

$$\bar{A}_n \approx \bar{B}_n = \frac{(n-1/2)!(-1)^n \zeta(\lambda - \eta - 2n\eta - 1)}{2^{n+3/2}n!(n+1)!\zeta(\lambda-1)} \tag{17}$$

and

$$A_n \approx B_n = \frac{(n-1/2)!(-1)^n \zeta(\lambda - \eta - 2n\eta)}{2^{n+3/2}n!(n+1)!\zeta(\lambda)}, \tag{18}$$

respectively. Using these formulas, the local field and the order parameter are determined by Eqs. (15) and (16). On the other hand, the generalized harmonic number H_m^q in general diverges when $0<q<1$ as $H_m^q \simeq (m+1)^{1-q}/(1-q)+\zeta(q)+O(m^{-q})$ in the $m\to\infty$ limit, which is shown in the Appendix. Here q is an index and represents $q=\lambda-\eta-2n\eta-1$ in Eq. (15), for example.

Equations (15) and (16) are divided into analytic and singular parts as

$$\bar{r} = \sum_n \bar{B}_n (J\bar{r})^{2n+1} + \bar{C}(J\bar{r}k_m^{\eta})(J\bar{r})^{(\lambda-2)/\eta} \tag{19}$$

and

$$r = \sum_n B_n (J\bar{r})^{2n+1} + C(J\bar{r}k_m^{\eta})(J\bar{r})^{(\lambda-1)/\eta}, \tag{20}$$

respectively, where the functions $\bar{C}(x)$ and $C(x)$ are defined in the Appendix. In the $x\to\infty$ limit corresponding to the thermodynamic limit, $\bar{C}(x)$ and $C(x)$ reduce to $\bar{C}_\infty$ and C_∞, respectively, defined as

$$\bar{C}_\infty = \frac{[(\lambda-2\eta-2)/2\eta]![(2-\lambda-\eta)/2\eta]!}{\eta 2^{(\lambda+4\eta-2)/2\eta}[(\lambda+\eta-2)/2\eta]!\zeta(\lambda-1)},$$

$$C_\infty = \frac{[(\lambda-2\eta-1)/2\eta]![(1-\lambda-\eta)/2\eta]!}{\eta 2^{(\lambda+4\eta-1)/2\eta}[(\lambda+\eta-1)/2\eta]!\zeta(\lambda)}. \quad (21)$$

Thus, the local field and the order parameter are written as

$$\bar{r} = \sum_{n=0}^{\infty} \bar{B}_n (J\bar{r})^{2n+1} + \bar{C}_\infty (J\bar{r})^{(\lambda-2)/\eta} + \cdots \quad (22)$$

and

$$r = \sum_{n=0}^{\infty} B_n (J\bar{r})^{2n+1} + C_\infty (J\bar{r})^{(\lambda-1)/\eta} + \cdots, \quad (23)$$

for $J\bar{r}k_m^\eta \gg 1$. We remark that the singular terms appear only in the limit $J\bar{r}k_m^\eta \to \infty$. For the case of $J\bar{r}k_m^\eta \ll 1$, however, Eqs. (15) and (16) are valid.

Next, we determine the critical point. To proceed, we investigate the behavior of the local field as a function of J, which depends on the sign of η.

(i) *In the case of* $\eta \leqslant 0$, $\bar{A}_n$ and A_n are finite. One can see from Eq. (15) that the local field is zero for $\bar{A}_0 J < 1$ and nonzero for $\bar{A}_0 J > 1$. The order parameter behaves in the same manner as that of the local field from Eq. (16). Thus, we obtain the critical point as

$$J_c = \frac{1}{\bar{A}_0} = J_0 \frac{H_{k_m}^{\lambda-1}}{H_{k_m}^{\lambda-1-\eta}}, \quad (24)$$

where $J_0 = 2\sqrt{2}/\sqrt{\pi}$. This formula can be written in another form as

$$J_c = J_0 \frac{\langle k \rangle}{\langle k^{1+\eta} \rangle}. \quad (25)$$

As $\lambda \to \infty$, the critical point J_c approaches $J_0 \simeq 1.60$ in the limit $N \to \infty$, which is consistent with that found in the case of the globally coupled oscillators [10].

When $J > J_c$, the local field $\bar{r}$ and the order parameter r are nonzero. When J is close to J_c,

$$\bar{r} \simeq (|\bar{A}_1| J_c^3)^{-1/2} \Delta^{1/2} \quad (26)$$

and

$$r \simeq A_0 (|\bar{A}_1| J_c)^{-1/2} \Delta^{1/2}, \quad (27)$$

where $\Delta = (J - J_c)/J_c$. Thus, we obtain that $\beta = 1/2$. Again, this result is consistent with the one obtained from the globally coupled oscillators [10].

(ii) *In the case of* $\eta > 0$, the singular terms in Eqs. (22) and (23) can be crucial in determining the critical point and the order parameter. Depending on relative magnitude of λ and η, we divide the case of $\eta > 0$ into four subcases:

(I) When $0 < \eta < (\lambda-2)/3$ (i.e., $\lambda > 3\eta+2$), $\bar{r} \simeq \bar{B}_0 J\bar{r} + \bar{B}_1 J^3 \bar{r}^3 + \cdots$ for small $\bar{r}$ from Eq. (22). Then J_c and $\bar{r}$ behave as those for $\eta < 0$ presented in Eqs. (24) and (26).

(II) When $(\lambda-2)/3 < \eta < \lambda-2$ (i.e., $\eta+2 < \lambda < 3\eta+2$), the dominant contribution is made from the singular term of Eq. (22). Then

$$\bar{r} \simeq \bar{B}_0 J\bar{r} + \bar{C}_\infty (J\bar{r})^{(\lambda-2)/\eta} + \cdots, \quad (28)$$

leading to

$$J_c \simeq 1/\bar{B}_0 = J_0 \frac{\zeta(\lambda-1)}{\zeta(\lambda-\eta-1)} \quad (29)$$

and

$$\bar{r} \sim r \sim \Delta^{\eta/(\lambda-2-\eta)}. \quad (30)$$

(III) When $\lambda-2 < \eta < \lambda-1$ (i.e., $\eta+1 < \lambda < \eta+2$), the critical point in Eq. (24) for finite N behaves as

$$J_c \sim k_m^{-(\eta-\lambda+2)} \sim N^{-(\eta-\lambda+2)/(\lambda-1)}. \quad (31)$$

Thus, it approaches zero in the thermodynamic limit. $\bar{r}$ is always positive unless J is zero as $\bar{r} \sim J^{(\lambda-2)/(\eta-\lambda+2)}$ for small J and $r \sim J\bar{r} \sim J^{\eta/(\eta-\lambda+2)}$.

(IV) When $\eta > \lambda-1$ (i.e., $\lambda < \eta+1$), we obtain that $r \sim (J\bar{r})^{(\lambda-1)/\eta}$. Using the result of $\bar{r}$ obtained in (III), we obtain that

$$r \sim J^{(\lambda-1)/(\eta-\lambda+2)}. \quad (32)$$

We summarize the result as follows: When $\eta < \lambda-2$ [in the (I) and (II) cases], the critical point J_c is finite; however, when $\eta > \lambda-2$ [in the (III) and (IV) cases], $J_c = 0$ in the thermodynamic limit $N \to \infty$. Thus, the critical exponent β associated with the order parameter is defined through the relation, $r \sim \Delta^\beta$ ($r \sim J^\beta$) for the former (latter) case. The exponent β is evaluated in each case as follows:

$$\beta = \begin{cases} 1/2 & \text{in (I)}, \\ \eta/(\lambda-2-\eta) & \text{in (II)}, \\ \eta/(\eta-\lambda+2) & \text{in (III)}, \\ (\lambda-1)/(\eta-\lambda+2) & \text{in (IV)}. \end{cases} \quad (33)$$

Our result implies that the nature of the synchronization transition depends on the parameter η controlling the coupling strength. This is counterintuitive from the perspective of the traditional concept of universality in critical phenomenon theory. The critical point J_c also depends on the parameter η as shown explicitly in Eq. (25). This is a generalization of the previous one with $\eta = 1$, $J_c = J_0 \langle k \rangle / \langle k^2 \rangle$, derived in [11–13]. This is also closely related to the percolation threshold [17] in complex networks. Moreover, the result $\beta = 1/2$ for $\eta = 1$ and $\lambda > 5$ is reduced to the mean-field result in Euclidean space.

IV. CLUSTER FORMATION OF SYNCHRONIZED OSCILLATORS

In this section, we investigate in detail how the coupled oscillator system develops its synchrony as the coupling strength increases. To this end, we study the formation of clusters comprising synchronized vertices as a function of the coupling strength J. We use the generating function approach to derive the cluster-size distribution.

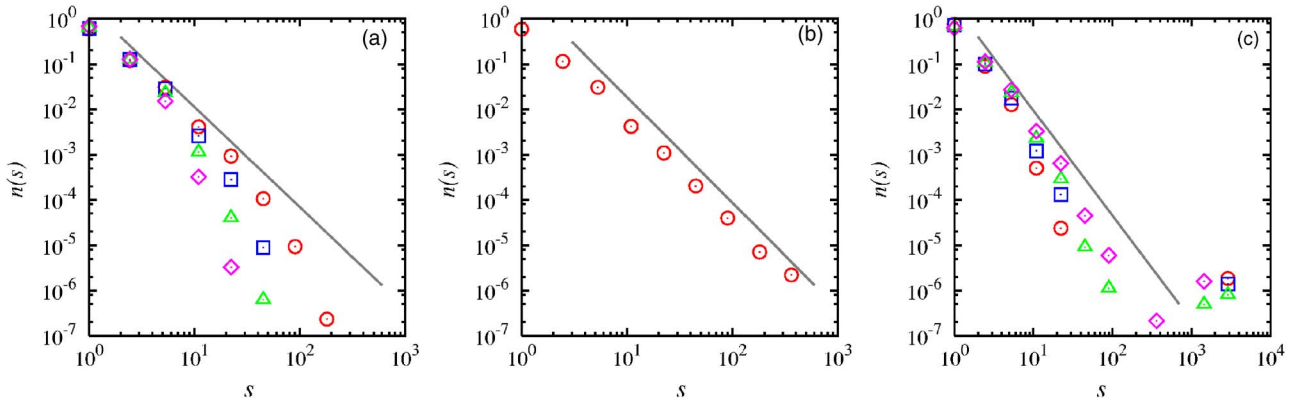

FIG. 1. (Color online) The size distributions $n(s)$ of synchronized clusters for the networks generated with $\lambda=4.0$, $\eta=0.0$, and $N=3000$ at $J=J_c$. Two neighboring vertices are regarded as being coherent when C_{ij} defined in Eq. (36) is larger than C. C is taken as 0.670 (○), 0.680 (□), 0.690 (△), and 0.700 (◇) in (a). Those values of C are larger than the critical value $C_{\text{th}}\approx 0.663$, which is taken in (b). In (c), C is taken as being smaller than C_{th} as 0.640 (○), 0.645 (□), 0.650 (△), and 0.655 (○). The data in (a), (b), and (c) show subcritical, critical, and supercritical behaviors, respectively. Solid lines drawn for reference have a slope of 7/3 for all.

A. Cooperative versus background synchrony

The order parameter averaged over the natural frequency distribution $g(\omega)$ can be written as

$$r = \frac{1}{N}\sqrt{\sum_i \langle \cos^2\phi_i + \sin^2\phi_i\rangle + \sum_i \sum_{j\neq i} \langle \cos(\phi_i - \phi_j)\rangle} \tag{34}$$

from Eq. (4). Here, the angular brackets represent the average over $g(\omega)$. For the case of $J=0$, each element oscillates independently, so that $\langle\cos(\phi_i-\phi_j)\rangle=0$ for $i\neq j$. Thus, the order parameter is evaluated as

$$r_{J=0} \sim \frac{1}{\sqrt{N}}. \tag{35}$$

As J increases, clusters comprising synchronized oscillators are more likely to form. We here define a cluster as a group of vertices (or oscillators) which are connected and in the same coherent state: Two oscillators are regarded as being coherent if its time-average correlation function C_{ij}, defined as

$$C_{ij} = \frac{1}{(t_1 - t_0)} \sum_{t=t_0+1}^{t_1} \langle \cos[\phi_i(t) - \phi_j(t)]\rangle, \tag{36}$$

is larger than a preassigned threshold value C. Such connected and coherent vertices form a cluster. When C is chosen as $C\approx 1$ (0), average cluster size becomes small (large). We find that there exists a critical value C_{th} at J_c, by which the cluster-size distribution follows a power law. As such clusters form, the term of $\Sigma_i\Sigma_{j\neq i}\langle\cos(\phi_i-\phi_j)\rangle$ becomes nonzero. The order parameter is then evaluated as

$$r \sim \frac{\sqrt{\sum_\kappa s_\kappa^2}}{N}, \tag{37}$$

where κ is the index of cluster and s_κ is the size of cluster κ—i.e., the number of vertices within the cluster κ. Note that $\Sigma_\kappa s_\kappa = N$ and Eq. (37) reduces to Eq. (35) when $J=0$ because each cluster size is 1. When $J \geqslant J_c$, the size of the largest cluster, denoted as S, is dominant and $\Sigma_\kappa s_\kappa^2 \approx S^2$, and thus the order parameter is approximately given as

$$r \sim S/N. \tag{38}$$

It is noteworthy that the parameter $1-C$ may be seen as the occupation probability p_{perc} in percolation theory. Thus, for $C > C_{\text{th}}$ ($C < C_{\text{th}}$), the cluster-size distribution shows a subcritical (critical) behavior and, at C_{th}, it shows the critical behavior. This is shown in Figs. 1(a)–1(c) where the cluster-size distributions for various values of C are shown at $J=J_c\approx 1.53$ for a network with parameters shown in the figure caption. One may wonder the logic of finding C_{th}. Unfortunately, we cannot determine C_{th} analytically; however, it is important to notice that such a critical point exists indeed and can be found numerically as shown in Fig. 1(b). This is analogous to finding the percolation threshold as the value of p_{perc} where the cluster-size distribution follows a power law, rather than the value where the order parameter of the percolation transition becomes nonzero. C_{th} depends on J. Here, however, since we are mainly interested in the asymptotic behavior of the cluster-size distribution at the critical point J_c, we find C_{th} numerically at J_c only.

Next, we study the cluster-size distribution as a function of J with the given C_{th} determined at J_c. For small $J<J_c$ (for large $J>J_c$), the cluster-size distribution shows a subcritical (supercritical) behavior. The exponent τ describing the power-law behavior at $J=J_c$ depends on the parameters η and λ. We determine τ using the generating function method in the next subsection.

B. Generating function of the cluster-size distribution

The probability that a vertex belongs to a cluster with size s is given by $sn(s)/N$, which is denoted as $p(s)$. Invoking percolation theory, $p(s)$ follows a power law with an exponential cutoff,

$$p(s) \sim s^{1-\tau} e^{-s/s_c}, \tag{39}$$

where s_c is the characteristic size, which depends on J and system size N. In the thermodynamic limit $N \to \infty$, s_c diverges at $J=J_c$. As in the percolation theory, the generating function $\mathcal{P}(z) \equiv \Sigma_s p(s) z^s$ is useful for studying structural feature of the synchronized clusters, since its singular behavior is related to the critical behavior of the synchronization transition. (i) The order parameter $r \sim S/N$ can be obtained from the relation $r = \lim_{N\to\infty}[1-\mathcal{P}(z_N^*)]$, where $\mathcal{P}(z_N^*) = \Sigma_{s<S} p(s)$—i.e., the contribution by finite-size clusters. This can be achieved by choosing $z_N^* \approx e^{-1/S_m}$, where S_m is a cluster size smaller than the largest cluster but larger the second largest cluster. (ii) From Eq. (39), one can find that $\mathcal{P}(z)$ diverges for $z > z_c = \lim_{s\to\infty} p(s)^{-1/s}$—i.e., $z_c \approx e^{1/s_c}$. Thus, at $J=J_c$, $\mathcal{P}(z) \sim (1-z)^{\tau-2}$ as $z \to z_c = 1$ in the thermodynamic limit. Thus, finding the singularity of $\mathcal{P}(z)$ enables one to obtain $p(s)$.

For this purpose, we introduce another generating function $\bar{\mathcal{P}}(z)$ as a partner of the local field $\bar{r}$. From $\bar{\mathcal{P}}(z)$, one can define a probability $\bar{p}(s)$ via the relation $\bar{\mathcal{P}}(z) \equiv \Sigma_s \bar{p}(s) z^s$, where $\bar{p}(s)$ is defined similarly to $p(s)$ as the probability that a vertex belongs to a synchronized cluster of size s composed of the vertex and $s-1$ neighboring vertices. For finite N, the generating function $\bar{\mathcal{P}}(z)$ is analytic for $|z| \leqslant 1$ and so is its inverse function $\bar{\mathcal{P}}^{-1}(z)$. To investigate the singularity of $\bar{\mathcal{P}}(z)$ near $z=1$, we consider the expansion of the inverse function $z = \bar{\mathcal{P}}^{-1}(\omega) = 1 - \Sigma_{n\geqslant 1} b_n (1-\omega)^n$ around $\omega = 1$. The coefficient b_n depends on J. Using Eqs. (15) and (22) and replacing $\bar{r}$ by $1-\omega$, we can find that the generating function $\bar{\mathcal{P}}(z)$ satisfies the self-consistent relations

$$z = \bar{\mathcal{P}}(z) + \sum_{n=0}^{\infty} \bar{B}_n \{J[1-\bar{\mathcal{P}}(z)]\}^{2n+1} + \bar{C}_\infty \{J[1-\bar{\mathcal{P}}(z)]\}^{(\lambda-2)/\eta} + \cdots, \tag{40}$$

for $J(1-\bar{\mathcal{P}}(z))k_m^\eta \gg 1$, and

$$z = \bar{\mathcal{P}}(z) + \sum_{n=0}^{\infty} \bar{A}_n \{J[1-\bar{\mathcal{P}}(z)]\}^{2n+1}, \tag{41}$$

for $J(1-\bar{\mathcal{P}}(z))k_m^\eta \ll 1$. Similarly, $\mathcal{P}(z)$ is determined as

$$z - \mathcal{P}(z) = \sum_{n=0}^{\infty} B_n \{J[1-\bar{\mathcal{P}}(z)]\}^{2n+1} + C_\infty \{J[1-\bar{\mathcal{P}}(z)]\}^{(\lambda-1)/\eta} + \cdots, \tag{42}$$

for $J[1-\bar{\mathcal{P}}(z)]k_m^\eta \gg 1$, and

$$z - \mathcal{P}(z) = \sum_{n=0}^{\infty} A_n \{J[1-\bar{\mathcal{P}}(z)]\}^{2n+1}, \tag{43}$$

for $J[1-\bar{\mathcal{P}}(z)]k_m^\eta \ll 1$.

C. Behavior of $p(s)$ at the critical point

Here, we calculate the probability $p(s)$ to find a vertex in the s-size cluster at the critical point $J=J_c$ explicitly in each case defined in Sec. III.

In case (I), since $\eta < (\lambda-2)/3$, we obtain that $z = 1 + \bar{B}_1 \{J_c[1-\bar{\mathcal{P}}(z)]\}^3 + \cdots$ to leading order by expanding $z = \bar{\mathcal{P}}^{-1}(\omega)$ around $\omega = 1$ in either Eq. (40) or (41). Thus, we obtain that $1-\bar{\mathcal{P}}(z) \sim (1-z)^{1/3}$, leading to

$$\bar{p}(s) \sim s^{-4/3} \tag{44}$$

for large s.

Using the obtained leading behaviors of $\bar{\mathcal{P}}(z)$ around $z=1$ in Eqs. (42) and (43), one obtains the behavior of $\mathcal{P}(z)$ around $z=1$ as $1-\mathcal{P}(z) \sim (1-z)^{1/3}$: thus,

$$p(s) \sim s^{-4/3}. \tag{45}$$

In case (II), the singular term in Eq. (40) is relevant. In this case, the behavior of $\bar{\mathcal{P}}(z)$ for $z < z_c$ differs from that for $z > z_c$. z_c is determined by the criterion $J[1-\bar{\mathcal{P}}(z_c)]k_m^\eta \sim 1$. This case also happens for cases (III) and (IV).

In this case, the singular term $\bar{C}_\infty \{J_c[1-\bar{\mathcal{P}}(z)]\}^{(\lambda-2)/\eta}$ is dominant in Eq. (40); therefore, it follows that $1-\bar{\mathcal{P}}(z) \sim J_c^{-1}(1-z)^{\eta/(\lambda-2)}$ at $J=J_c$, which is valid for $z \gg z_c$. From this result, $\bar{p}(s)$ is obtained as

$$\bar{p}(s) \sim J_c^{-1} s^{-(\eta+\lambda-2)/(\lambda-2)}, \tag{46}$$

which is valid for $s \ll s_c$.

On the other hand, when $J[1-\bar{P}(z)]k_m^\eta \ll 1$ so that $|\bar{A}_{n+1}/\bar{A}_n|[J(1-\bar{P}(z))]^2 \ll 1$, one can obtain that $1-\bar{\mathcal{P}}(z) \sim J_c^{-1}|\bar{A}_1|^{-1/3}(1-z)^{1/3}$ for $z \ll z_c$; therefore,

$$\bar{p}(s) \sim J_c^{-1} k_m^{(\lambda-2)/3-\eta} s^{-4/3} \tag{47}$$

for large $s \gg s_c$. s_c is evaluated as follows: Substituting the result of $1-\bar{\mathcal{P}}(z)$ in the criterion $J_c[1-\bar{\mathcal{P}}(z_c)]k_m^\eta \sim 1$ and using $(1-z_c) \sim s_c^{-1}$, one can obtain a system-size dependence of the characteristic size s_c explicitly as

$$s_c \sim k_m^{\lambda-2} \sim N^{(\lambda-2)/(\lambda-1)}, \tag{48}$$

which diverges as $N \to \infty$ when $\lambda > 2$.

Together with Eqs. (46) and (47), we obtain that

$$\bar{p}(s) \sim \begin{cases} s^{-(\eta+\lambda-2)/(\lambda-2)} & (s \ll s_c), \\ k_m^{(\lambda-2)/3-\eta} s^{-4/3} & (s \gg s_c). \end{cases} \tag{49}$$

Next, using the result of $1-\mathcal{P}(z) \sim 1-\bar{\mathcal{P}}(z)$ obtained from both Eqs. (42) and (43), one can find that $p(s)$ behaves similarly to $\bar{p}(s)$: that is,

$$p(s) \sim \begin{cases} s^{-(\eta+\lambda-2)/(\lambda-2)} & (s \ll s_c), \\ k_m^{(\lambda-2)/3-\eta} s^{-4/3} & (s \gg s_c). \end{cases} \tag{50}$$

In case (III), the critical point J_c is finite in finite-size systems as being of order $J_c \sim k_m^{\lambda-2-\eta} \sim N^{(\lambda-2-\eta)/(\lambda-1)}$. Plugging the N dependence into Eq. (47) and the expression $1-\bar{\mathcal{P}}(z) \simeq 1-z+\bar{C}_\infty[J_c(1-z)]^{(\lambda-2)/\eta}$ for $s \ll s_c$ from Eq. (40), one obtains $\bar{p}(s)$ as follows:

$$\bar{p}(s) \sim \begin{cases} k_m^{(\lambda-2-\eta)(\lambda-2)/\eta} s^{-(\lambda-2+\eta)/\eta} & (s \ll s_c), \\ k_m^{-2(\lambda-2)/3} s^{-4/3} & (s \gg s_c). \end{cases} \tag{51}$$

Next, we derive $p(s)$. We find that the leading singular term in $\mathcal{P}(z)$ for the case $1-z \gg s_c^{-1} \sim k_m^{2-\lambda}$ shows up in two ways. Substituting $1-\overline{\mathcal{P}}(z) \approx 1-z+\bar{C}_\infty[J_c(1-z)]^{(\lambda-2)/\eta}$ into Eq. (42), we obtain that $1-\mathcal{P}(z) \approx B_0 J_c(1-z)+B_0 J_c \bar{C}_\infty[J_c(1-z)]^{(\lambda-2)/\eta}+C_\infty[J_c(1-z)]^{(\lambda-1)/\eta}+\cdots$. We compare the second with the third terms in order of magnitude. Using the fact that $J_c \sim k_m^{\lambda-2-\eta}$, we find that there exist two subcases for $s \ll s_c$. The second term $B_0 J_c \bar{C}_\infty[J_c(1-z)]^{(\lambda-2)/\eta}$ is more dominant than the third term $C_\infty[J_c(1-z)]^{(\lambda-1)/\eta}$ when $1-z \ll s_*^{-1}$ and vice versa. Here, it is found that a new crossover size s_* scales as

$$s_* \sim k_m^{(\eta-1)(\eta-\lambda+2)}. \tag{52}$$

From the behaviors of $\mathcal{P}(z)$ in the three different subcases, we obtain the probability $p(s)$ as

$$p(s) \sim \begin{cases} k_m^{(\lambda-1)(\lambda-2-\eta)/\eta} s^{-(\lambda-1+\eta)/\eta} & (s \ll s_*), \\ k_m^{(\lambda-2-\eta)(\lambda-2+\eta)/\eta} s^{-(\lambda-2+\eta)/\eta} & (s_* \ll s \ll s_c), \\ k_m^{(\lambda-2)/3-\eta} s^{-4/3} & (s \gg s_c). \end{cases} \tag{53}$$

One can notice that the subcase $s \ll s_*$ diminishes when $\eta \leqslant 1$, but it is extended as the parameter η increases.

In case (IV), the third term $C_\infty[J_c(1-z)]^{(\lambda-1)/\eta}$ in $1-\mathcal{P}(z)$ in case (III) is always dominant when $1-z \gg s_c^{-1}$. Moreover, A_0 in Eq. (43) diverges as $A_0 \sim k_m^{\eta-\lambda+1}$, which has to be considered in the relation $1-\bar{P}(z) \simeq A_i J_c(1-\bar{P}(z))$ for $1-z \ll s_c^{-1}$. Consequently, $p(s)$ behaves as

$$p(s) \sim \begin{cases} k_m^{(\lambda-1)(\lambda-2-\eta)/\eta} s^{-(\lambda-1+\eta)/\eta} & (s \ll s_c), \\ k_m^{(1-2\lambda)/3} s^{-4/3} & (s \gg s_c). \end{cases} \tag{54}$$

To substantiate the predictions of this section, we investigate the asymptotic behavior of $p(s)$ in a numerical manner. The static model introduced in [19] is used for the underlying network in our simulations. The network has $N=3000$ oscillators and its mean degree $\langle k \rangle$ is 4.0. The values of λ and η are chosen as 4.0 and 0.0, respectively. This pair belongs to case (I). First, we simulate the system at $J=J_c$ to determine C_{th} defined in Sec. IV A. During the simulation, we assume a large value of C_{th} and then collect the pairs of vertices where the C_{ij} of each pair is larger than the assumed C_{th}. After that, we determine clusters and obtain the cluster-size distribution. We then adjust C_{th} by somewhat decreasing or increasing it and repeat these procedures until the power-law distribution appears in the cluster-size distribution. If the cluster-size distribution follows the power-law form of $n(s) \sim s^{-\tau}$, the corresponding value of C_{th} is considered as the threshold value C_{th}. It is found numerically that $C_{\text{th}} \approx 0.66$, independent of the system size N. In our simulations, we obtain $\tau \approx 7/3$, which is close to the theoretical value in Eq. (45), as shown in Fig. 1(b).

V. LARGEST CLUSTER SIZE AND FINITE-SIZE SCALING

In this section, we first investigate the N dependence of the largest cluster size at J_c. Next, based on this result, we derive a finite-size scaling form for the order parameter near J_c.

A. Largest cluster size

The largest cluster size S can be obtained from the relation

$$\sum_{s>S} p(s) \sim \frac{S}{N}. \tag{55}$$

In case (I), we use the result of Eq. (45) and obtain simply that

$$S \sim N^{3/4}. \tag{56}$$

In case (II), $p(s)$ displays a crossover at s_c, and thus the obtained value of the largest cluster size must satisfy the self-consistency conditions. For instance, the largest cluster size obtained by Eq. (55) for $s \ll s_c$ in Eq. (50) has to be smaller than s_c. As a result, the largest cluster size behaves differently in the two subcases $\eta<1$ and $\eta \geqslant 1$, which we denote (IIa) and (IIb), respectively. In each subcase, we obtain that

$$S \sim \begin{cases} N^{(4\lambda-5-3\eta)/[4(\lambda-1)]} & \text{in (IIa)}, \\ N^{(\lambda-2)/(\lambda-2+\eta)} & \text{in (IIb)}. \end{cases} \tag{57}$$

The largest cluster size S in (IIa) was determined from $p(s)$ for $s \gg s_c$ and is indeed much larger than s_c, whereas it in (IIb) was done from $p(s)$ for $s \ll s_c$.

In case (III), $p(s)$ exhibits three distinct power-law behaviors. Thus, this case is divided into three subcases. They are as follows: $\eta<1$ (IIIa), $1 \leqslant \eta \leqslant \sqrt{\lambda^2-3\lambda+3}$ (IIIb), and $\eta > \sqrt{\lambda^2-3\lambda+3}$ (IIIc). The largest cluster size in each subcase is given as

$$S \sim \begin{cases} N^{(4\lambda-5-3\eta)/[4(\lambda-1)]} & \text{in (IIIa)}, \\ N^{\eta/(\lambda-2+\eta)+(\lambda-2-\eta)/(\lambda-1)} & \text{in (IIIb)}, \\ N^{(\lambda-2)/(\lambda-1+\eta)} & \text{in (IIIc)}. \end{cases} \tag{58}$$

In case (IV), the largest cluster size is determined simply by $p(s)$ for $s \ll s_c$ since the resulting largest cluster size fulfills the criterion $S<s_c$ for $\eta>0$: thus,

$$S \sim N^{(\lambda-2)/(\lambda-1+\eta)}. \tag{59}$$

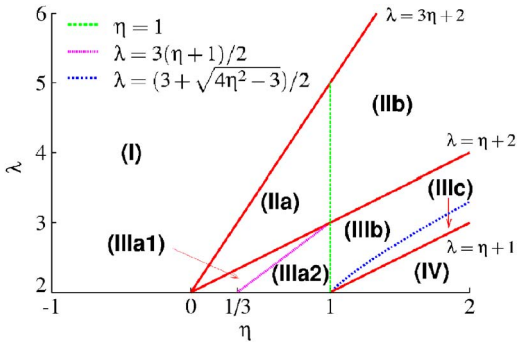

FIG. 2. (Color online) Diagram in the space of (η,λ) of eight different domains, each corresponding to a distinct synchronization transition. The transition nature of each domain is listed in Table I.

TABLE I. The probability to find a vertex in s-size cluster $p(s)$, the critical exponents β and μ, and the largest cluster size S at the critical point for the eight cases shown in Fig. 2.

domain	$p(s)$	β	μ	S
(I)	$s^{-4/3}$	$\frac{1}{2}$	2	$N^{3/4}$
(II)	$\begin{cases} s^{-(\eta+\lambda-2)/(\lambda-2)} & (s \ll s_c), \\ k_m^{(\lambda-2)/3-\eta} s^{-4/3} & (s \gg s_c) \end{cases}$	$\frac{\eta}{\lambda-2-\eta}$	$\frac{\eta}{1+3\eta}\frac{4(\lambda-1)}{\lambda-2-\eta}$ (IIa) $\frac{\lambda-2+\eta}{\lambda-2-\eta}$ (IIb)	$N^{(4\lambda-5-3\eta)/[4(\lambda-1)]}$ (IIa) $N^{(\lambda-2)/(\lambda-2+\eta)}$ (IIb)
(III)	$\begin{cases} k_m^{(\lambda-1)(\lambda-2-\eta)/\eta} s^{-(\lambda-1+\eta)/\eta} & (s \ll s_*) \\ k_m^{(\lambda-2-\eta)(\lambda-2+\eta)/\eta} s^{-(\lambda-2+\eta)/\eta} & (s_* \ll s \ll s_c) \\ k_m^{(\lambda-2)/3-\eta} s^{-4/3} & (s \gg s_c). \end{cases}$	$\frac{\eta}{\eta-\lambda+2}$	$\frac{\eta}{1+3\eta}\frac{4(\lambda-1)}{\eta-\lambda+2}$ (IIIa1) $\frac{2\eta}{\eta-\lambda+2}$ (IIIa2, IIIb, IIIc)	$N^{(4\lambda-5-3\eta)/[4(\lambda-1)]}$ (IIIa1, IIIa2) $N^{\eta/(\lambda-2+\eta)+(\lambda-2-\eta)/(\lambda-1)}$ (IIIb) $N^{(\lambda-2)/(\lambda-1+\eta)}$ (IIIc)
(IV)	$\begin{cases} k_m^{(\lambda-1)(\lambda-2-\eta)/\eta} s^{-(\lambda-1+\eta)/\eta} & (s \ll s_c) \\ k_m^{(1-2\lambda)/3} s^{-4/3} & (s \gg s_c). \end{cases}$	$\frac{\lambda-1}{\eta-\lambda+2}$	$\frac{2(\lambda-1)}{\eta-\lambda+2}$	$N^{(\lambda-2)/(\lambda-1+\eta)}$

B. Finite-size scaling

Here, we evaluate the magnitude of the order parameter r_c at J_c and establish the finite-size scaling function. To proceed, we compare the magnitude of cooperative synchrony S/N with that of the background synchrony $\sim N^{-1/2}$. The order parameter r_c is defined as $\sim S/N$ if $S/N \gg N^{-1/2}$ and $\sim N^{-1/2}$ otherwise. Under this criterion, we obtain r_c as $\sim S/N$ in cases (I) and (II) and $\sim N^{-1/2}$ in cases (IIIb), (IIIc), and (IV). Case (IIIa) is divided into two subcases $2\lambda-3\eta-3 \geqslant (<) 0$. They are denoted as (IIIa1) and (IIIa2), respectively. The order parameter r_c behaves as $\sim S/N$ and $\sim N^{-1/2}$ in (IIIa1) and (IIIa2), respectively.

By using that $r \sim \Delta^{\beta}$ and N-dependent behavior of r_c at J_c, we can construct a finite-size scaling form as

TABLE II. Numerical values of the parameters (η,λ) we used for Fig. 3. β_t and μ_t are theoretical values for a given set of (η,λ) in the third column. β_n and μ_n are numerical values to draw Fig. 3 for each case. For (a)-(c), the theoretical and numerical values are the same each other for both β and μ. However, they can be different for (d)-(h). r_t and r_n are the order parameters in scaling form formulated with the theoretical values of β_t and μ_t and the numerical values β_n and μ_n, respectively.

Fig. 3	domain	(η,λ)	β_t	β_n	μ_t	μ_n	r_t	r_n
(a)	(I)	(1/3,4)	1/2	1/2	2	2	$N^{-1/4}\psi(\Delta N^{1/2})$	$N^{-1/4}\psi(\Delta N^{1/2})$
(b)	(IIa)	(5/6,4)	5/7	5/7	120/49	120/49	$N^{-7/24}\psi(\Delta N^{49/120})$	$N^{-7/24}\psi(\Delta N^{49/120})$
(c)	(IIb)	(4/3,4)	2	2	5	5	$N^{-2/5}\psi(\Delta N^{1/5})$	$N^{-2/5}\psi(\Delta N^{1/5})$
(d)	(IIIa1)	(1/3,13/6)	2	20/7	14/3	20/3	$N^{-3/7}\psi(JN^{3/14})$	$N^{-3/7}\psi(JN^{3/20})$
(e)	(IIIa2)	(2/3,13/6)	4/3	50/23	8/3	100/23	$N^{-1/2}\psi(JN^{3/8})$	$N^{-1/2}\psi(JN^{23/100})$
(f)	(IIIb)	(5/2,4)	5	5	10	10	$N^{-1/2}\psi(JN^{1/10})$	$N^{-1/2}\psi(JN^{1/10})$
(g)	(IIIc)	(11/4,4)	11/3	11/3	22/3	22/3	$N^{-1/2}\psi(JN^{3/22})$	$N^{-1/2}\psi(JN^{3/22})$
(h)	(IV)	(4,4)	3/2	5	3	10	$N^{-1/2}\psi(JN^{1/3})$	$N^{-1/2}\psi(JN^{1/10})$

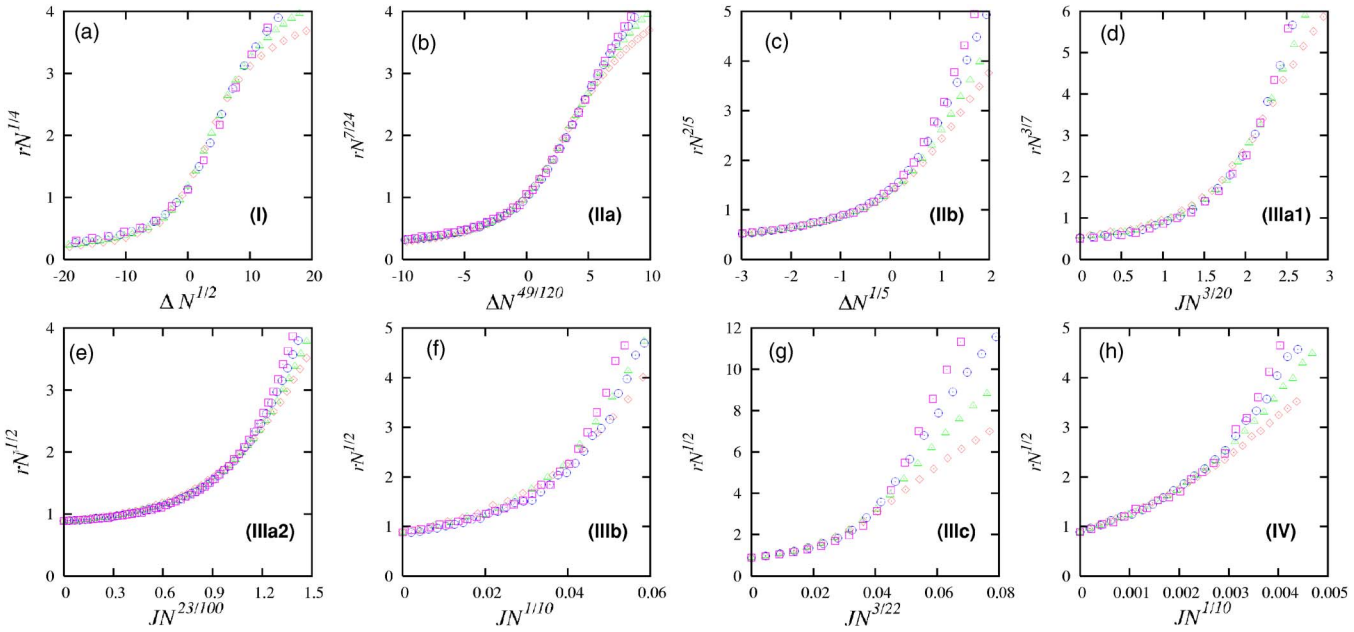

FIG. 3. (Color online) Finite-size scaling behaviors of the order parameter r. Data are collected from the static network model with mean degree $\langle k\rangle=4$ and system sizes $N=400$ ($\diamond$), 800 ($\triangle$), 1600 ($\bigcirc$), and 3200 ($\square$). Numerical values of the tunable parameters (η,λ) and the critical exponents are given in Table II for each case. For the critical point J_c, theoretical $J_c^{(t)}$, and numerical $J_c^{(n)}$ values used in (a)–(c) are different as $(J_c^{(t)},J_c^{(n)})=(0.92,1.32)$ (a), (0.37,0.50) (b), and (0.13,0.18) (c).

$$r = N^{-\beta/\mu}\psi(\Delta N^{1/\mu}) \tag{60}$$

for cases (I) and (II) and

$$r = N^{-\beta/\mu}\psi(JN^{1/\mu}) \tag{61}$$

for cases (III) and (IV), where

$$\psi(x) \sim \begin{cases} \text{const} & \text{for } x \ll 1, \\ x^{\beta} & \text{for } x \gg 1. \end{cases} \tag{62}$$

The critical exponent μ is determined by the relation $r_c \sim N^{-\beta/\mu}$. The value of μ varies depending on the cases determined by the magnitude of η and λ.

We present the diagram in Fig. 2 comprising eight distinct cases in the (η,λ) plane. Each case in the diagram corresponds to a distinct behavior of the critical exponents β and μ, the cluster-size distribution, and the largest cluster size. We summarize those features in Table I.

VI. NUMERICAL SIMULATIONS

We perform direct numerical integration of Eq. (2) to confirm the analytic results. In particular, the finite-size scaling behaviors in Eqs. (60) and (61) are compared. For this purpose, we generate random SF networks using the static model [19] with system sizes of $N=400$, 800, 1600, and 3200, mean degree of $\langle k\rangle=4.0$, and values of η and λ chosen from each domain in Fig. 2. The numerical values of (λ,η) we used are listed in Table II. For the numerical integration, we apply Heun's method [20]. Time is discretized by a unit step $\delta t=0.005$ and runs up to $t=1.2\times10^4$. An ensemble average is taken over $O(10^2)\sim O(10^3)$ different configurations of natural frequencies and network realizations, respectively.

Numerical results are presented in Fig. 3. For each Figure 3(a)–3(c), the critical point J_c is finite. We find J_c numerically to make the obtained numerical data collapsed for different system size N in the scaling plot with theoretical values of β and μ. The theoretical and numerically found values of J_c, denoted as $J_c^{(t)}$ and $J_c^{(n)}$, respectively, are compared as $(J_c^{(t)},J_c^{(n)})\approx(0.92,1.32)$ for (a), (0.37, 0.50) for (b), and (0.13, 0.18) for (c). They belong to cases (I), (IIa), and (IIb), respectively. The theoretical values were obtained by using Eq. (25). However, when the generalized harmonic numbers $H_{k_m}^{\lambda-1}$ and $H_{k_m}^{\lambda-1-\eta}$ in Eq. (24) or the zeta functions $\zeta(\lambda-1)$ and $\zeta(\lambda-\eta-1)$ in Eq. (29) are used, the critical points are changed as $J_c^{(t)}\approx1.49$ (a), 1.27 (b), and 0.90 (c). The critical point is a nonuniversal quantity and sensitive to the method one uses, which was noticed in [13]. On the other hand, the discrepancy between the numerical value and the mean-field solution for the critical point was encountered in another problem. For example, Dorogovtsev *et al.* [15] studied the Ising model on a Cayley-tree-type structure and obtained an analytic solution of the critical point, which turned out to be larger than the mean-field solution, but closer to the numerical value.

For Figs. 3(d)–3(h), the critical point J_c is zero. For the cases of (d), (e), and (h), we find that numerical data do not collapse well in the scaling plot of $rN^{\beta/\mu}$ versus $JN^{1/\mu}$ with theoretical values of β_t and μ_t tabulated in Table I. Instead, we adjust the numerical values of β_n and μ_n values empirically to make the obtained numerical data collapsed. Those empirical values of β_n and μ_n are compared with the theo-

retical values as listed in Table II. The discrepancy in (d) and (e) originates from the presence of intrinsic degree-degree correlation in the static model when the degree exponent $2<\lambda<3$, while the theoretical values were obtained under the assumption that the degree-degree correlation is absent.

VII. CONCLUSIONS AND DISCUSSION

In this paper, we have investigated the nature of the synchronization transition generated by N limit-cycle oscillators located at random SF networks with degree exponent λ. The dynamics is given by a modified Kuramoto equation with the asymmetric and degree-dependent weighted coupling strength in the form of $Jk_i^{1-\eta}$, where k_i is the degree of vertex i. Depending on the sign and magnitude of η, the influence of the hub vertices on the dynamics can be moderated or amplified and determines the nature of the synchronization transition. Applying the mean-field approach to the modified Kuramoto equation, we derived the critical point, the size distribution of synchronized clusters, and the largest cluster size at the critical point. The critical exponents associated with the order parameter and the finite-size scaling are determined in terms of the two tunable parameters (η,λ). All results are summarized in Table. I. The parameter space of (η,λ) is divided into eight different domains, in each of which the transition nature is distinct.

It would be interesting to notice that the critical exponents β and μ associated with the order parameter and the finite-size scaling of the synchronization transition depend on the parameter η used to control the coupling strength. The result is unusual from the perspective of the universality in the critical phenomena in regular lattices where the details of the couplings are mostly irrelevant unless they are long ranged [21]. When the coupling constant depends on a strength of the long-ranged interaction in Euclidean space, the critical exponent can depend on the exponent controlling that strength, which is reminiscent of our result. Another implication of our result is that in scale-free networks where a long-ranged interaction is naturally involved, structural features of SF networks such as the degree distribution are not sufficient to understand the dynamic process in SF networks. As we have shown in this paper, asymmetric coupling in dynamics is a relevant perturbation in such networks due to the heterogeneity of the degree distribution. Such a behavior was also observed in the sandpile model [22]. The relevance of the asymmetric coupling could be used in other subjects—for example, improving the transport of data packet in the Internet [23] and enhancing the biomass product in metabolic networks [24], and so on.

ACKNOWLEDGMENTS

This work was supported by KRF Grant No. R14-2002-059-010000-0 of the ABRL program funded by the Korean government (MOEHRD) and the Seoul R&BD program.

APPENDIX: DERIVATION OF EQS. (19) and (20)

In this appendix, we present the derivation of Eqs. (19) and (20) from Eqs. (15) and (16) with $\eta>0$. Since the right-hand side of Eq. (16) becomes the same as that of Eq. (15) when λ is shifted by 1, we here analyze in detail the nature of Eq. (15) only, which applies also to Eq. (16) with λ replaced by $\lambda+1$.

The coefficients in Eq. (15) diverge with increasing N for $n\geqslant n_c\equiv\lceil(\lambda-\eta-2)/(2\eta)\rceil$, where $\lceil x\rceil$ is the smallest integer not smaller than x, due to the divergence of the generalized harmonic number H_m^q for $0<q<1$. While $H_m^q\simeq\zeta(q)$ for $q>1$, H_m^q diverges in the limit $m\to\infty$ for $0<q<1$ and its asymptotic expansion can be obtained by using the relation $H_m^q=\zeta(q)-\zeta(q,m+1)$ and the asymptotic expansion of the Hurwitz zeta function [25]

$$\zeta(q,m)=\frac{1}{q-1}m^{1-q}+\frac{1}{2}m^{-q}+2m^{1-q}\int_0^\infty dx\frac{\sin(q\tan^{-1}x)}{(1+x^2)^{q/2}(e^{2\pi mx}-1)}. \quad \text{(A1)}$$

One can see that the integral is of order m^{-1} in the limit $m\to\infty$ since

$$\int_0^\infty dx\frac{\sin(q\tan^{-1}x)}{(1+x^2)^{q/2}(e^{2\pi mx}-1)}\leqslant\int_0^{1/m}dx\frac{qx}{e^{2\pi mx}-1}+\int_{1/m}^\infty dx\frac{1}{e^{2\pi mx}-1}\simeq O(m^{-2})+O(m^{-1}), \quad \text{(A2)}$$

and thus for $0<q<1$, H_m^q behaves as

$$H_m^q=\sum_{k=1}^m\frac{1}{k^q}\simeq\frac{(m+1)^{1-q}}{1-q}+\zeta(q)+O(m^{-q}). \quad \text{(A3)}$$

When $\eta>0$, the terms with such diverging coefficients exist and thus we can rearrange the expansion as follows:

$$\begin{aligned}\bar{r}&=\sum_{n=0}^\infty\frac{(n-1/2)!(-1)^n(J\bar{r})^{2n+1}H_{k_m}^{\lambda-\eta-2n\eta-1}}{2^{n+3/2}n!(n+1)!\zeta(\lambda-1)}\\&=\sum_{n=0}^\infty\frac{(n-1/2)!(-1)^n\zeta(\lambda-\eta-2\eta n-1)}{2^{n+3/2}n!(n+1)!\zeta(\lambda-1)}(J\bar{r})^{2n+1}\\&\quad+\sum_{n=n_c}^\infty\frac{(n-1/2)!(-1)^nk_m^{2+\eta+2n\eta-\lambda}(J\bar{r})^{2n+1}}{2^{n+3/2}n!(n+1)!(2+\eta+2n\eta-\lambda)\zeta(\lambda-1)} \quad \text{(A4)}\\&=\sum_{n=0}^\infty\bar{B}_n(J\bar{r})^{2n+1}+(J\bar{r})^{(\lambda-2)/\eta}\bar{C}(J\bar{r}k_m^\eta), \quad \text{(A5)}\end{aligned}$$

where we approximated $H_{k_m}^{\lambda-1}$ by $\zeta(\lambda-1)$ since $\lambda-1>1$. The coefficients $\bar{B}_n$ are defined in Eq. (17), and the function $\bar{C}(x)$ is defined by

$$\bar{C}(x) = \sum_{n=n_c}^{\infty} \bar{c}_n x^{(2+\eta+2n\eta-\lambda)/\eta}, \tag{A6}$$

with

$$\bar{c}_n = \frac{(n-1/2)!(-1)^n}{2^{n+3/2} n!(n+1)!(2+\eta+2n\eta-\lambda)\zeta(\lambda-1)}.$$

While $\bar{C}(x)$ behaves as $x^{(2+\eta-\lambda+2\eta n_c)/\eta}$ for $x \ll 1$, it converges to a constant $\bar{C}_\infty$ for $x \to \infty$, yielding a nonanalytic term $\bar{C}_\infty (J\bar{r})^{(\lambda-2)/\eta}$ as can be seen in Eq. (22). Therefore, the magnitude of $J\bar{r}k_m^n$ is essential for the determination of the leading behaviors of the right-hand sides of Eqs. (15) and (16) for $\bar{r} \ll 1$. If $J\bar{r}k_m^\eta \gg 1$, one can approximate the function $\bar{C}(J\bar{r}k_m^\eta)$ by a constant $\bar{C}_\infty$ which is evaluated as

$$\begin{aligned}
\bar{C}_\infty &= \lim_{x\to\infty} \sum_{n=n_c}^{\infty} \frac{(n-1/2)!(-1)^n 2^{-(\lambda+2\eta-2)/(2\eta)}}{n!(n+1)!(2+\eta+2n\eta-\lambda)\zeta(\lambda-1)} \\
&\quad \times (2^{-1/2}x)^{(2+\eta+2n\eta-\lambda)/\eta} \\
&= \frac{1}{2^{(\lambda+2\eta-2)/(2\eta)}\zeta(\lambda-1)} \sum_{n=n_c}^{\infty} \frac{(-1)^n (n-1/2)!}{n!(n+1)!} \\
&\quad \times \int_0^\infty dy y^{1+\eta+2n\eta-\lambda} \\
&= \frac{[(\lambda-2\eta-2)/2\eta]![(2-\lambda-\eta)/2\eta]!}{\eta 2^{(\lambda+4\eta-2)/2\eta}[(\lambda+\eta-2)/2\eta]!\zeta(\lambda-1)}.
\end{aligned} \tag{A7}$$

The function $C(x)$ defined in the text can be approximated in the same way by a constant C_∞, which is identical to $\bar{C}_\infty$ with $\lambda+1$ in place of λ. Therefore, one should refer to Eqs. (22) and (23) for the correct expansions of r and $\bar{r}$ around $\bar{r}=0$ in the case of $J\bar{r}k_m^\eta \gg 1$ while Eqs. (15) and (16) can be used in the case of $J\bar{r}k_m^\eta \ll 1$.

[1] A. S. Pikovsky, M. G. Rosenblum, and J. Kurths, *Synchronization—A Universal Concept in Nonlinear Sciences* (Cambridge University Press, Cambridge, England, 2001); S. Boccaletti, J. Kurths, G. Osipov, D. L. Valladares, and C. S. Zhou, Phys. Rep. **366**, 1 (2002).

[2] M. Barahona and L. M. Pecora, Phys. Rev. Lett. **89**, 054101 (2002).

[3] H. Hong, M. Y. Choi, and B. J. Kim, Phys. Rev. E **65**, 026139 (2002).

[4] D. J. Watts and S. H. Strogatz, Nature (London) **393**, 440 (1998).

[5] A.-L. Barabási and R. Albert, Science **286**, 509 (1999).

[6] T. Nishikawa, A. E. Motter, Y.-C. Lai, and F. C. Hoppensteadt, Phys. Rev. Lett. **91**, 014101 (2003).

[7] A. E. Motter, C. Zhou, and J. Kurths, Phys. Rev. E **71**, 016116 (2005).

[8] M. Chavez, D.-U. Hwang, A. Amann, H. G. E. Hentschel, and S. Boccaletti, Phys. Rev. Lett. **94**, 218701 (2005).

[9] C. Zhou, A. E. Motter, and J. Kurths, Phys. Rev. Lett. **96**, 034101 (2006).

[10] Y. Kuramoto, *Chemical Oscillations, Waves and Turbulence* (Springer, Berlin, 1984). Y. Kuramoto, Prog. Theor. Phys. Suppl. **79**, 223 (1984).

[11] T. Ichinomiya, Phys. Rev. E **70**, 026116 (2004).

[12] D.-S. Lee, Phys. Rev. E **72**, 026208 (2005).

[13] J. G. Restrepo, E. Ott, and B. R. Hunt, Phys. Rev. E **71**, 036151 (2005).

[14] S. H. Strogatz, Physica D **143**, 1 (2000).

[15] S. N. Dorogovtsev, A. V. Goltsev, and J. F. F. Mendes, Phys. Rev. E **66**, 016104 (2002).

[16] D.-H. Kim, G. J. Rodgers, B. Kahng, and D. Kim, Phys. Rev. E **71**, 056115 (2005).

[17] R. Cohen, K. Erez, D. ben-Avraham, and S. Havlin, Phys. Rev. Lett. **85**, 4626 (2000); D. S. Lee, K.-I. Goh, B. Kahng, and D. Kim, Nucl. Phys. B **696**, 351 (2004).

[18] R. Pastor-Satorras and A. Vespignani, Phys. Rev. Lett. **86**, 3200 (2001).

[19] K.-I. Goh, B. Kahng, and D. Kim, Phys. Rev. Lett. **87**, 278701 (2001).

[20] J. Garcia-Ojalvo and J. M. Sancho, *Noise in Spatially Extended Systems* (Springer, New York, 1999).

[21] M. E. Fisher, S.-k. Ma, and B. G. Nickel, Phys. Rev. Lett. **29**, 917 (1972).

[22] K.-I. Goh, D.-S. Lee, B. Kahng, and D. Kim, Phys. Rev. Lett. **91**, 148701 (2003); D.-S. Lee, K.-I. Goh, B. Kahng, and D. Kim, J. Korean Phys. Soc. **44**, 633 (2004); Physica A **338**, 84 (2004).

[23] H. K. Lee, K.-I. Goh, B. Kahng, and D. Kim, e-print physics/0608163.

[24] E. Almaas *et al.*, Nature (London) **427**, 839 (2004); D. Segre *et al.*, Proc. Natl. Acad. Sci. U.S.A. **99**, 15112 (2002).

[25] D. Cvijovic and J. Klinowski, Math. Comput. **68**, 1623 (1999).